Spectral Dynamics of Spatially Incoherent Modulation Instability

Can Sun,[1] Laura Waller,[1] Dmitry V. Dylov,[1,2] and Jason W. Fleischer[1,3,*]

[1]*Department of Electrical Engineering, Princeton University, Princeton, New Jersey, 08544, USA*
[2]*General Electric Global Research Center, Niskayuna, New York 12309, USA*
[3]*Program in Applied and Computational Mathematics, Princeton University, Princeton, New Jersey 08544, USA*

(Received 30 November 2010; published 27 June 2012)

To date, all experiments in nonlinear statistical optics have relied on beams whose transverse spatial statistics were Gaussian. Here, we present a new technique to generalize these studies by using a spatial light modulator to create spatially incoherent beams with arbitrary spectral distributions. As a specific example of the new dynamics possible, we consider the spatial modulation instability of a partially coherent beam. We show that, for statistical beams of uniform intensity and equal correlation length, the underlying spectral shape determines the threshold and visibility of intensity modulations as well as the spectral profile of the growing sidebands. We demonstrate the behavior using statistical light, but the results will hold for any wave-kinetic system, such as plasma, ultracold gases, and turbulent acoustic waves.

DOI: 10.1103/PhysRevLett.108.263902 PACS numbers: 42.65.Sf, 05.45.−a, 52.35.−g

While the linear theory of statistical light propagation is nearly 50 years old [1,2], the nonlinear theory has been studied for little more than a decade [3–16]. As in the linear case, the initial results were generalizations of their coherent counterparts, this time provided by the seminal observations of random-phase solitons [3] and incoherent modulation instability [7]. Incoherent dynamics can be far richer, though, as it depends not only on the spatial profile of the beam but also on the spectral structure of its modes. For example, more general wave-kinetic dynamics were observed recently in the form of bump-on-tail instabilities [13] and spatial optical turbulence [14]. To date, however, only a limited number of distributions has been considered. More specifically, experiments done with spatially incoherent light have relied on quasithermal Gaussian distributions, while most theory has been performed for Lorentzian distributions. Other common distributions, such as quantum distributions and hyper-Lorentzian profiles [17], have not been explored for optical beams. Even more striking, relevant distributions within classical optics, such as fractal profiles [18] and natural image statistics [19], have not been considered either, a fact made more pressing by the recent discovery of instability-driven imaging [16]. Here, we use a spatial light modulator to experimentally create different spectral profiles and observe their corresponding nonlinear propagation. We use modulation instability as a particular example, but it is clear that the ability to change spectral distributions introduces a new degree of freedom into the study of nonlinear statistical dynamics, both within and beyond optics.

Modulation instability (MI) is a fundamental instability in which self-focusing perturbations extract energy from a broad-scale background, leading to the growth of small-scale perturbations. In coherent optics, for example, noise will immediately trigger the growth of modes, with the dominant spatial scale determined by a balance between nonlinearity and diffraction. For partially coherent light, perturbations have difficulty extracting energy from the incoherent background, as statistical dephasing competes with mode coupling. For distributions with smooth (differentiable) power spectra, there is a nonlinear threshold for instability [6,12].

Theoretically, several different theories have been proposed to describe the nonlinear propagation of partially coherent beams, all of which are equivalent [9]. Here, we use the mutual coherence function approach, which in the paraxial approximation is [5,6]

$$\frac{\partial f}{\partial z} - \frac{i}{k}\frac{\partial^2 f}{\partial r \partial \rho} = \frac{i n_0}{k}\left(\frac{\omega}{c}\right)^2 [\delta n(r_1, z) - \delta n(r_2, z)] f, \quad (1)$$

where $f(r_1, r_2, z) = \langle E^*(r_2, z, t) E(r_1, z, t)\rangle_t$ is the time-averaged mutual coherence function between two points r_1 and r_2, E is the slowly varying amplitude of the electric field, $r = (r_1 + r_2)/2$ is the center-of-mass coordinate, $\rho = r_1 - r_2$ is the separation coordinate, $k = \lambda/2\pi$ is the wave number for light of wavelength λ, n_0 is the base index of refraction, and δn is the nonlinear index change induced by the local light intensity $I = f(r_1, r_1, z)$.

We are interested in intensity modulations around a uniform background distribution. The envelope response can be considered perturbatively by linearizing Eq. (1) around an initially homogeneous intensity profile. For simplicity, we perform the calculations for an inertial Kerr medium with $\Delta n = \gamma \langle I\rangle_t$ (the case for the photorefractive nonlinearity, as used in the experiments, is similar). Reducing the system to one transverse dimension and writing $f(x, k_x, z) = f_0(k_x) + f_1 \exp[gz + i\alpha x]$ gives the dispersion relation [6]

$$1 = -k^2 \frac{\gamma}{n_0} \int_{-\infty}^{\infty} dk_x \frac{f_0(k_x + \frac{\alpha}{2}) - f_0(k_x - \frac{\alpha}{2})}{igk + \alpha k_x}. \quad (2)$$

The appropriate coherence function $f_0(k_x)$ can then be substituted and solved for the growth rate g for a particular perturbation mode α. For example, a Lorentzian distribution with a spectral spread of k_{x0}, $f = (I_0 k_{x0}/\pi)/({k_x}^2 + {k_{x0}}^2)$, allows Eq. (2) to be solved exactly, giving the dispersion relation [6]

$$g_{\text{Lorentzian}} = |\alpha| \left[-\frac{k_{x0}}{k} + \sqrt{\frac{\gamma I_0}{n_0} - \left(\frac{\alpha}{2k}\right)^2} \right]. \quad (3)$$

This expression shows clearly that the gain rate for coherent MI must overcome the statistical nature of the light, with a nonlinear threshold $\Delta n_{\text{th,Lorentzian}} = \gamma I_0 = n_0 (k_{x0}/k)^2$.

A similar result holds for a Gaussian distribution, $f(k_x) = I_0 \exp(-k_x^2/\bar{k}_{x0}^2)/\sqrt{\pi \bar{k}_{x0}^2}$ (where $\bar{k}_{x0} = k_{x0}\sqrt{\ln 2}$), used in all the experiments to date [7]. In this case, Eq. (2) cannot be solved exactly. However, for long-wavelength modulations, the spectral difference in the numerator can be approximated as $\alpha \partial_x f$ [10,11,13]. At the threshold for modulation instability, the growth rate $g = 0$, so that Eq. (2) gives [11]

$$\Delta n_{\text{th,Gaussian}} = \frac{n_0}{2} \left(\frac{\bar{k}_{x0}}{k}\right)^2 \approx 0.72 \Delta n_{\text{th,Lorentzian}}. \quad (4)$$

For distributions with the same total intensity and full width at half-maximum (FWHM), the Gaussian has a lower threshold for modulation instability than the Lorentzian. This is reasonable, since the Lorentzian distributes more modes at higher spatial frequencies than the Gaussian.

This intuition also holds for a uniform beam with a rectangular distribution, which contains all its modes within its FWHM. To see this explicitly, consider the profile given by $f_{\text{rectangular}}(k_x) = (I_0/2k_{x0})$ for $|k_x| \le k_{x0}$ and zero otherwise. This distribution also allows Eq. (2) to be solved exactly, resulting in the growth rate [12]

$$g^2_{\text{rectangular}} = \alpha^2 \left[-k_{x0}^2 - \frac{\alpha^2}{4} + \frac{\alpha k_{x0}}{\tanh(\alpha k_{x0} n_0/\gamma I_0)} \right]. \quad (5)$$

For any positive value of the nonlinearity, there always exists some finite wave number α for which the gain rate remains positive. Theoretically, there is no nonlinear threshold for instability, despite the statistical nature of the beam. In practice, the finite width of the medium gives a lower bound to the possible wave numbers, leading to an effective threshold for the observation of modulations.

From these results, the prevailing argument has been that distributions with smaller spectral tails give less competition for partially coherent MI. However, it is easy to show that this intuition is incorrect and that the dynamics are significantly more complex. To do this, we introduce an exponential distribution (the Fourier transform of the Lorentzian), $f(k_x) = (I_0/2k_{x0}) \exp[-\ln 2 |k_x/k_{x0}|]$, which is as smooth as the Lorentzian and Gaussian profiles but has spectral tails which lie between the two. This distribution does not yield an analytic solution to Eq. (3), but its threshold can again be obtained by approximating the numerator as $\alpha \partial_x f$ and setting $g = 0$; the result is

$$\Delta n_{\text{th,exponential}} = \frac{1}{\Gamma} \frac{n_0}{\ln(4)} \left(\frac{k_{x0}}{k}\right)^2 \approx 1.25 \cdot n_0 \cdot \left(\frac{k_{x0}}{k}\right)^2, \quad (6)$$

where $\Gamma \approx 0.577$ is the Euler constant. This threshold is the largest of all the cases, despite the fact that the Lorentzian has the most energy in the high-k modes and is therefore the "most statistical" of the distributions. This momentum measure is misleading, though, as the dispersion relation (and thus threshold value) of the instability is determined by an integral over the distribution. That is, it is not clear *a priori* which modes contribute the most to the dynamics. Since the FWHM is the same for all the distributions, as are the zeroth-order and first-order moments (total energy and center of mass, respectively), it was natural to attribute the differences to the tails [6,11,12]. On the other hand, very little energy is contained in the high-k modes. A better figure of merit, proposed here, is given by the second-order moment $\int_{-\Delta k}^{\Delta k} dk_x [k_x^2 f(k_x)] / \int_{-\Delta k}^{\Delta k} dk_x f(k_x)$, taken to be band-limited to provide convergence for the Lorentzian. While the choice $\Delta k = k_{x0}$ gives the correct threshold ordering, the choice $\Delta k = 2 \cdot k_{x0}$ gives a better numerical match: 0.79 for the Gaussian:Lorentzian ratio and 1.12 for the exponential:Lorentzian ratio, both of which are within 10% of their analytical values.

We now proceed to test these results experimentally. As mentioned above, all previous demonstrations of partially coherent modulation instability have been performed with Gaussian distributions. To remedy this, we use the setup shown in Fig. 1. The nonlinear medium is a $5 \times 5 \times 10$ mm photorefractive SBN:60 ($Sr_{0.6}Ba_{0.4}Nb_2O_6$) crystal,

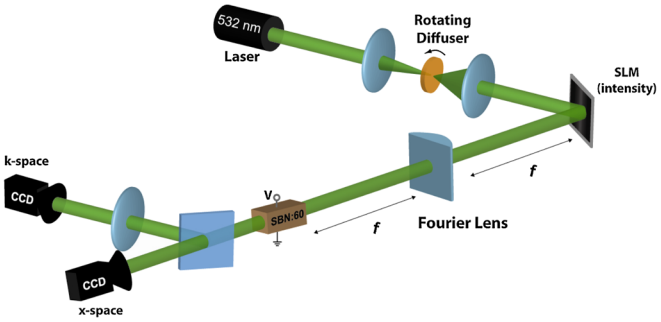

FIG. 1 (color online). Experimental setup. Light from a 532 nm laser is made partially spatially incoherent by passing it through a rotating diffuser. A spatial light modulator then reshapes the k-space spectrum before the beam is sent into a photorefractive SBN:60 crystal. Light exiting the crystal is imaged in both x space and k space.

and the beam is from a 532 nm laser, polarized extraordinarily to take advantage of the electro-optic coefficient $r_{33} = 235$ pm/V. The crystal has a slow time response (~ 1 s), due to photoexcited charge transport, with a nonlinearity that is controllable by a voltage bias applied across the crystalline c axis [4]. As in previous experiments, we make a statistical beam by focusing the light onto a diffuser that is rotated at a very fast rate (~ 200 Hz), so that the crystal sees only a time-averaged, quasithermal intensity. The diffused light is then imaged onto a spatial light modulator (SLM) so that it uniformly fills the array, which is used to redistribute the Gaussian profile into the desired spectral distribution. [While the SLM could create a statistical distribution by itself, this two-step process proved cleaner in the experiments, as the resulting phase fluctuations are faster than the SLM could provide (a refresh rate of $\sim$60 Hz)]. A cylindrical lens placed after the SLM is used to optically Fourier transform the modified spectrum onto the input plane of the crystal. The output intensity and spectral distribution are monitored using two CCD cameras: one in the near field (x space) and one in the Fourier domain (k space).

We consider the four spectral distributions described above: rectangular, Gaussian, Lorentzian, and exponential distributions. Numerical and experimental pictures of the spectral distributions are shown in Fig. 2. The four distributions are normalized to the same 15 μW total power and the same FWHM of 0.06 μm^{-1} [Figs. 2(a) and 2(c)]. In x space, the beams have a uniform intensity across the entire crystal face (so that the dark conductivity of SBN is minimal) [7] and are virtually indistinguishable. If one takes the spectral linewidth as a measure of the (transverse) correlation length, then each beam has the same spatial coherence properties. Alternatively, if one defines the spatial coherence length as the width of the two-point correlation function f_0 [Fig. 2(b)], then there is some subjectivity, as the curves drop off at different rates. However, all of the correlation curves intersect at a two-point separation distance of 16 μm (consistent with the spectral FWHM), when the visibility $[(I_{\max} - I_{\min})/(I_{\max} + I_{\min})]$ is 10%. Accordingly, we take this value as the experimental metric for the onset of MI.

To observe modulation instability, we increase the nonlinearity by applying a voltage across the crystalline c axis. Figure 3(a) shows intensity images in x space at the output face of the crystal as a function of applied voltage. At 300 V, the beam with a rectangular spectrum has already developed visible modulations while the beams with other distributions show no signs of modulation. By 600 V, the Gaussian distribution is beginning to break up but the beams with Lorentzian and exponential spectra remain flat. These latter spectra only began to display visible modulations above 1200 V.

Cross sections of the intensity modulations are shown in Fig. 3(b), showing the growth of perturbations with increasing nonlinearity (voltage). In all but the rectangular distribution at the highest voltages, the modulations retain the sinusoidal form of linearized theory. This signifies that higher-order terms in the crystal response, such as saturation [4,6,7] and nonlocality [20], do not play a significant role for most of the observations. Indeed, numerical simulations of Eq. (1) (using a split-step beam propagation code

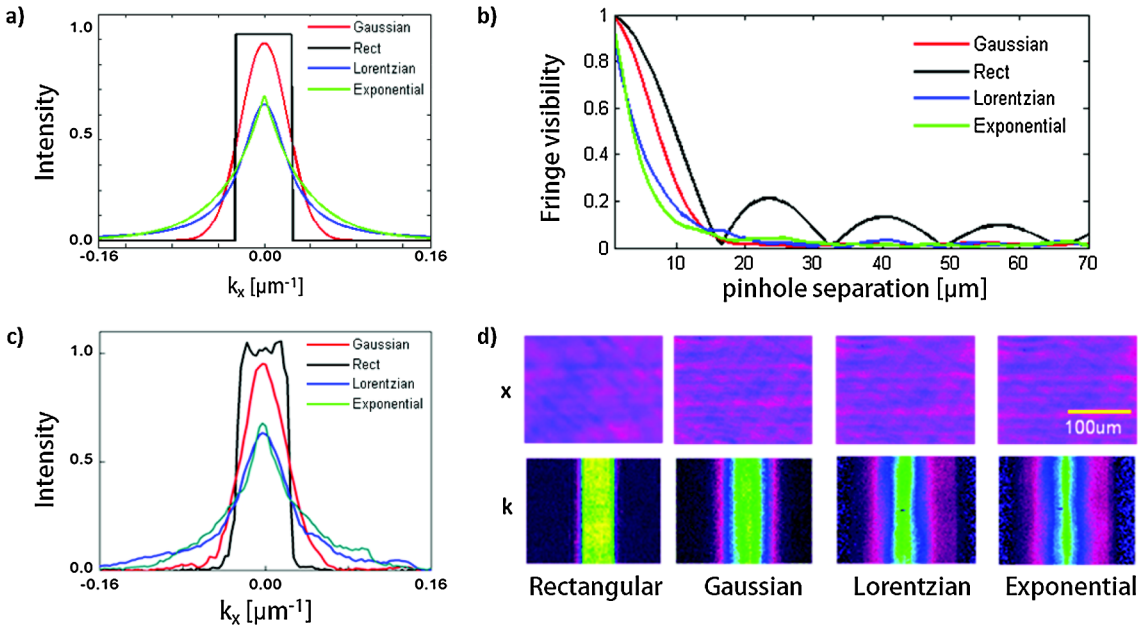

FIG. 2 (color online). Conditions at the input plane of a crystal. (a),(c) Cross sections of (a) simulated and (c) experimental Fourier spectra. (b) Numerical plot of two-point fringe visibility describing spatial coherence; (d) x space and k space of rectangular, Gaussian, Lorentzian, and exponential beams at input.

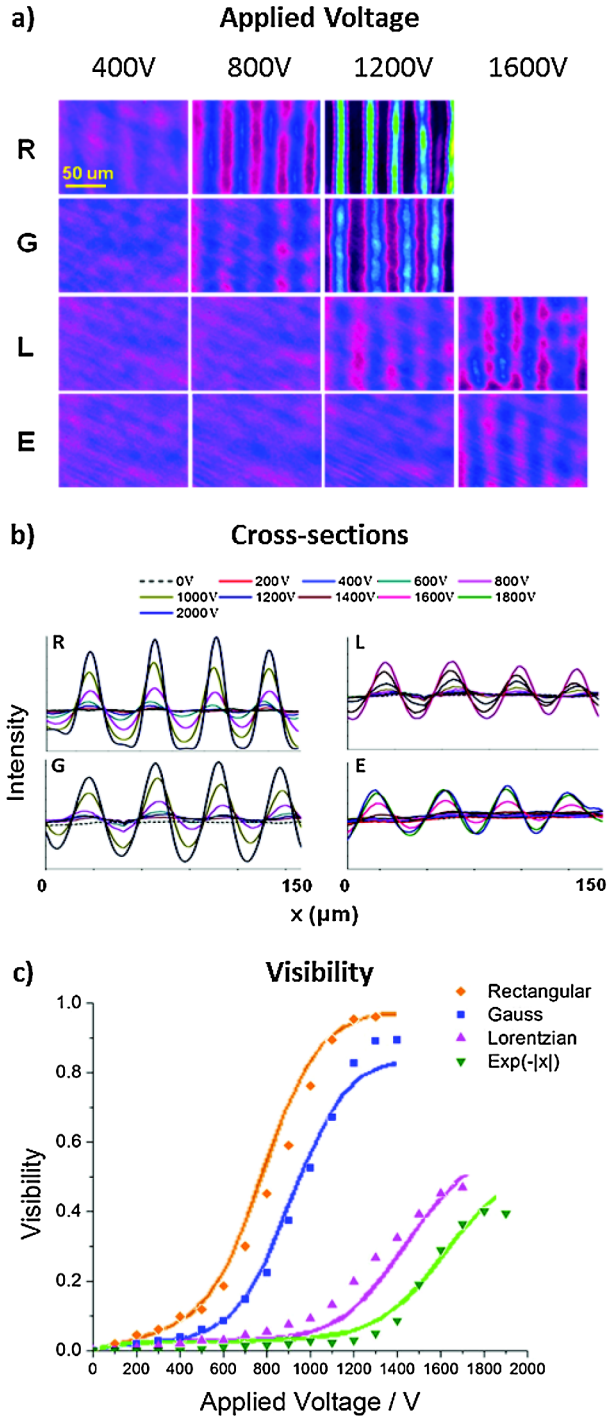

FIG. 3 (color online). Experimental results. (a) Intensity images at the output plane of a crystal for different nonlinearities (applied voltages) and different spectra (R, rectangular; G, Gaussian; L, Lorentzian; E, exponential). (b) Cross sections and (c) visibility of intensity modulations. The solid lines in (c) show simulations of the expected behavior using a beam propagation code.

with 1000 interacting modes) with only a Kerr nonlinearity show reasonable agreement with the experiment [Fig. 3(c)].

As a measure of the instability threshold, we record the nonlinearity needed for the modulations to achieve a visibility of 10%. The thresholds for the rectangular, Gaussian, Lorentzian, and exponential are approximately 600, 800, 1200, and 1600 V, respectively. As predicted, the Lorentzian has a higher threshold than the Gaussian. Experimentally, the ratios of $\Delta n_{\mathrm{th,Gaussian}}/\Delta n_{\mathrm{th,Lorentzian}}$ and $\Delta n_{\mathrm{th,Lorentzian}}/\Delta n_{\mathrm{th,exponential}}$ are 0.67 and 1.33, respectively, in good accord with the theoretical values of 0.72 and 1.25. For the beam with a rectangular spectrum, which has been predicted to have no instability threshold, small modulations were visible at low voltages, even though we have defined its threshold to be at 300 V.

Plots of the visibility of intensity modulations are shown in Fig. 3(c). In addition to the obvious differences in thresholds, the plots show clearly the differences in maximum visibility achieved by each beam, which are nontrivial to calculate theoretically. The rectangular spectrum achieves the highest visibility, followed by the Gaussian, Lorentzian, and the exponential distributions, an ordering which is consistent with the threshold behavior.

Having confirmed that x-space evolution is strongly dependent on the spectral distribution, we now study how different spectral distributions affect the evolution of the spectral function itself. Intensity pictures of the Fourier spectrum for the rectangular and Gaussian distributions are shown in Fig. 4(a), along with cross sections at different nonlinearities. It is clear from the figures that the spectral distributions of the sidebands are simply scaled versions of the main profile. To support this, we vary the width of the rectangular spectrum; as shown in Fig. 4(b), the sidebands continue to be rectangularly shaped, with their widths matching the width of the initial distribution almost exactly. While the initial matching is intuitive, as the scaling follows directly from linearized perturbation theory, its persistence into the strongly nonlinear regime is surprising.

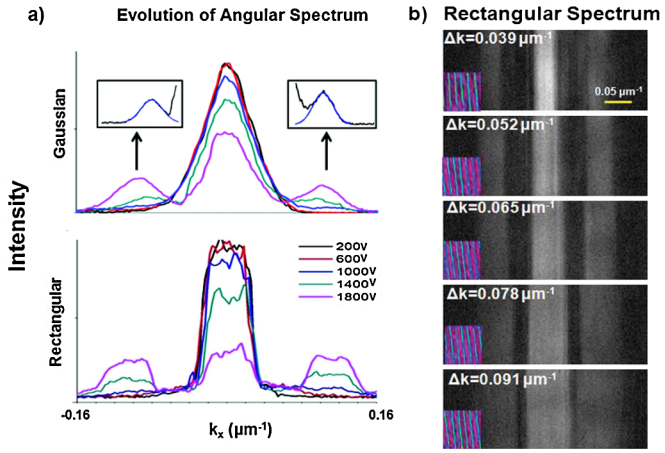

FIG. 4 (color online). Evolution of angular spectrum. (a) Evolution as a function of nonlinearity (applied voltage) for Gaussian and rectangular distributions. The insets show fits to Gaussians. (b) Angular spectrum at the output plane for a rectangular spectrum at the same nonlinearity for different widths of the initial spectrum. Inset: real-space intensity.

To the best of our knowledge, this correspondence has not been predicted previously.

In conclusion, we have experimentally demonstrated the dependence of spatially incoherent modulation instability on the underlying spectral distributions. Behavior is significantly different for beams with the same intensity and correlation lengths but different shapes of their spectral distributions. These shapes determine both the nonlinear threshold for modulations and the spectral profiles of the growing sidebands. Even though we have looked at modulation instability in particular, the results and experimental setup open the door to all spectral and phase-space phenomena in nonlinear statistical optics.

*jasonf@princeton.edu

[1] E. Wolf, Proc. R. Soc. A **230**, 246 (1955).
[2] A. Blanc-Lapierre and P. Dumontet, Rev. Phys. Appl. **34**, 1 (1955).
[3] M. Mitchell, Z. G. Chen, M. F. Shih, and M. Segev, Phys. Rev. Lett. **77**, 490 (1996).
[4] D. N. Christodoulides, T. H. Coskun, M. Mitchell, and M. Segev, Phys. Rev. Lett. **78**, 646 (1997).
[5] V. V. Shkunov and D. Z. Anderson, Phys. Rev. Lett. **81**, 2683 (1998).
[6] M. Soljacic, M. Segev, T. Coskun, D. N. Christodoulides, and A. Vishwanath, Phys. Rev. Lett. **84**, 467 (2000).
[7] D. Kip, M. Soljacic, M. Segev, E. Eugenieva, and D. N. Christodoulides, Science **290**, 495 (2000).
[8] R. Fedele and D. Anderson, J. Opt. B **2**, 207 (2000).
[9] D. N. Christodoulides, E. D. Eugenieva, T. H. Coskun, M. Segev, and M. Mitchell, Phys. Rev. E **63**, 035601 (2001).
[10] B. Hall, M. Lisak, D. Anderson, R. Fedele, and V. E. Semenov, Phys. Rev. E **65**, 035602 (2002).
[11] D. Kip, M. Soljacic, M. Segev, S. M. Sears, and D. N. Christodoulides, J. Opt. Soc. Am. B **19**, 502 (2002).
[12] D. Anderson, L. Helczynski-Wolf, M. Lisak, and V. Semenov, Phys. Rev. E **69**, 025601 (2004).
[13] D. V. Dylov and J. W. Fleischer, Phys. Rev. Lett. **100**, 103903 (2008).
[14] D. V. Dylov and J. W. Fleischer, Phys. Rev. A **78**, 061804 (2008).
[15] C. Sun, D. V. Dylov, and J. W. Fleischer, Opt. Lett. **34**, 3003 (2009).
[16] D. V. Dylov and J. W. Fleischer, Nature Photon. **4**, 323 (2010).
[17] R. M. Thorne and D. Summers, Phys. Fluids B **3**, 2117 (1991).
[18] H. Funamizu and J. Uozumi, Opt. Express **15**, 7415 (2007).
[19] A. Torralba and A. Oliva, Netw., Comput. Neural Syst. **14**, 391 (2003).
[20] W. Krolikowsi, O. Bang, J. J. Rasmussen, and J. Wyller, Phys. Rev. E **64**, 016612 (2001).